Computer simulation of evaporative cooling storage system performance

William A. Olosunde[1,*], Ademola K. Aremu[2], Paul Okoko[1]

(1. Department of Agricultural and Food Engineering, Faculty of Engineering, University of Uyo, Uyo, Nigeria
2. Department of Agricultural and Environmental Engineering, Faculty of Technology, University of Ibadan, Ibadan, Nigeria)

Abstract: Evaporative cooling occurs when warm and unsaturated air is blown across a wet surface. This study reviews the development of simulation software as a research tool for designing evaporative cooling systems. The simulation incorporates information concerning the effect of the cooling pad length, cooling pad height, cooling pad thickness, air velocity, water flow rate, water temperature, water to air mass flow rate, and number of cooling pad segments in terms of the performance efficiency of the cooling system. The software rapidly produced model data, which was subjected to further analysis for verification and validation during the testing stage. The modelled and experimental data of the saturation efficiency were compared using 4 of the most important statistical parameters, based on a paired sample t-test of an equal variance assumption. The results indicated that there was no significant difference between the software generated data and the experimental data of the Saturation Efficiency on Pad Thickness – mm ($p = 0.635$), Air Velocity - m/s ($p = 0.140$), Water Flow Rate - L/min ($p = 0.341$) and Water Temperature °C ($p = 0.567$) at $\alpha = 0.05$ significance level and 95% confidence interval.

Keywords: evaporative cooling system, saturation efficiency modelled data simulation, t-test

Citation: Olosunde, W. A., A. K. Aremu, and P. Okoko. 2016. Computer simulation of evaporative cooling storage system performance. Agricultural Engineering International: CIGR Journal, 18(4):280-292.

1 Introduction

In view of its simplicity and relative efficiency, evaporative cooling offers high potential for use in the preservation of fruits and vegetables. Evaporative cooling is an environmental-friendly and energy saving technology for air conditioning (Cui et al., 2014). Ndukwu and Manuwa (2014) provided a detailed description of evaporative cooling.

A mathematical model for a direct evaporative cooling air conditioning system was developed by Camargo et al. (2003). Kachhwaha and Suhas (2010) performed a heat and mass transfer study in a direct evaporative cooler. Considerable attention has been devoted to the design and construction of a simple evaporative cooling system.

Evaporative cooling occurs when warm and unsaturated air is blown across a wet surface. The sensible heat of the air is converted into latent heat to change the water from liquid to vapour. Thus, the air is cooled by losing its sensible heat and is humidified due to the added vapour released into the air stream (Ndukwu, 2011; Dzivama, 2000).

Designing pad and fan cooling systems requires fundamental knowledge of moist air properties, (psychrometrics), the air velocity through the pad, the water flow rate onto the pad and the evaporative pad operational characteristics (Dzivama, 2000). Two Microsoft Windows based digital psychrometric chart tools have been developed. These are entitled ‘psyc’ written in Visual C++ (Fang et al., 2001), and ‘psychart’, written in MATLAB (Wang et al., 2001). These programs are highly useful as teaching and research tools. Thus,

Received date: 2016-07-22 **Accepted date:** 2016-09-10
***Corresponding author: William A. Olosunde,** Department of Agricultural and Food Engineering, Faculty of Engineering, University of Uyo, Uyo, Nigeria. Email: williamolosunde@uniuyo.edu.ng

this new software system was developed for a pad and fan system used in a storage chamber for the storage of fruits and vegetables. The primary objective of this research was to develop a software script using the MATLAB programming language to design an entire Adiabatic Cooling System, considering the heat and mass balance exchange inside the storage chamber, and the psychrometric variables.

2 Materials and methods

The system was based on MATLAB R2011a software installed on a local laptop computer. The software was written using an M-file programming Script together with a graphical user interface and powerful toolboxes provided by MATLAB. The heat and mass exchanges were simulated considering the permanent conditions inside the storage chamber. The activity at the pad-end involves heat and mass transfer processes, which can be approximated using the wet-bulb thermometer analysis as presented by Olosunde (2015), Taye and Olorunisola (2011), Kulkarni and Rajput (2011) and Dzivama (2000). These processes can be expressed by mathematical formulae, linking measurable input parameters to obtain measurable output parameters. The output parameters are temperature, relative humidity and the saturation efficiency of the air leaving the pad after the evaporative cooling process.

2.1 Mathematical modelling

The mathematical model used in this work, although based on other different mathematical theories and evaluation, was developed in such a way that the variable parameters were kept dynamic to allow for users to provide input with the aim of optimizing the data for an efficient performance of the evaporative cooling system. Olosunde (2015) and Van der Walt and Hemp (1989) described the steady-state heat balance and temperature on a wet thermometer as Equation 1:

$$h_c (Tdb-Twb) + F_{ev} h_r (MRT-Twb) = h_c \lambda 0.7 (e_s-e)/P \quad (1)$$

where *Tdb* is the dry bulb temperature ℃, *Twb* is the wet bulb temperature ℃, h_c is the convective heat transfer coefficient W/(m^2.K), *Fev* is the view factor for the bulb (typically 0.8) with respect to its surrounding radiation field. The view factor should be combined with the emissivity of the bulb, which is typically approximately 0.95, with the combined view and emissivity factor being 0.74, *MRT* is the mean radiant temperature, ℃.

2.1.1 Saturation efficiency (SE)

Saturation efficiency (SE), which is an important criterion to judge an evaporative cooling system, is calculated as a temperature difference ratio using Equation 2 (Olosunde et al., 2009; Xuan et al., 2012; Sirelkhatim and Emad 2012):

$$SE = (Tdb - Tc) / (Tdb - Twb) \quad (2)$$

where *Tc* is the storage chamber temperature, ℃

2.1.2 Storage chamber model

In modelling and simulating an evaporative cooling system to attain an optimum cooling temperature for fruits and vegetables and to optimize the design of the system itself, some parameters were made dynamic to fit the user's environmental conditions in order to obtain an efficient cooling temperature after simulation. These include the storage chamber length, storage chamber width, storage chamber height, cooling pad length, cooling pad height, and cooling pad thickness.

The followings are the sources of heat loads of the cooler determined using the model:

(i) Heat gain by conduction, through the walls, roof and floor of the cooler.

The heat transfer by conduction into the store was calculated by multiplying the area of the various components of the cooler, such as the walls, floor and roof, by their appropriate conductivity value, i.e., the reciprocal of the insulation thickness, and by the difference between the outside and inside air temperatures (Equation 3). The total was obtained by the addition of these various products.

$$Q = KA\frac{dT}{dt} \quad (3)$$

where Q is the heat transfer by conduction, W, A is the total area of the various components, m^2, dT is the difference between the outside and inside temperatures, ℃ and dt is the insulation thickness, m.

(ii) Respiration heat load of the produce.

The respiration heat can be expressed as Equation 4:

$$Q_r = M_P \times P_r \quad (4)$$

where Q_r is the respiration heat, W/h, M_P is the mass of the produce, kg, P_r = rate of respiration heat production, W/kg h.

(iii) Field heat of the produce.

The field heat is the heat acquired by the produce in the field. The field heat is expressed as Equation 5:

$$Q_f = (M_P C_P)\Delta T/t_c \quad (5)$$

where Q_f is the field heat acquired by the produce, W, C_P is the specific heat capacity of the produce, kJ/kg ℃, t_c is the cooling time in s, (for fruits it is equal to 12 h), ΔT is the change in temperature (Olosunde et al., 2009; Boyette et al., 2010; Ndukwu et al., 2013).

(iv) Infiltration of air.

This heat is estimated to arise from 10% – 20% of the total heat load from other sources (Olosunde et al., 2009). Thus taking an average of 15%, this produces as Equation 6:

$$Q_L = (Q_c + Q_f + Q_r) \times 15/100 = (Q_c + Q_f + Q_r) \times 0.15 \quad (6)$$

where Q_L is the heat transfer through the cracks and the opening of the cooler door.

2.1.3 Heat and mass balance for the pad-end model

Figure 1 depicts the pad-end model for which the heat and mass balance are derived. The change in the sensible heat q is equal to the change in the enthalpy h_c of the air after passing through the pad. The Equation 7 is given by:

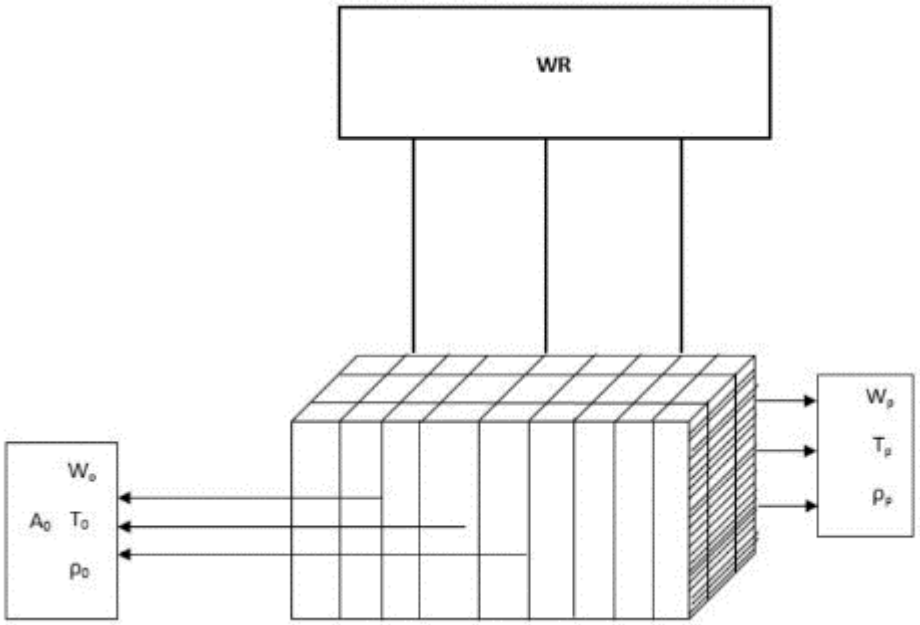

Figure 1 Pad end model

$$dT/dP_T = \frac{h^1(T_{0(db)} - T_p)}{\rho_a V_a C_a + \rho_a V_a W_0 C_v} \quad (7)$$

The rate of evaporation M_T could be expressed as Equation 8:

$$M_T = h_D \rho_a V_a (H_p - H_o) P_p P_A / V_a$$
$$= (h_D \rho_a V_a M_w)/(R_o T_{abs}) \times (P_{vs} - P_{va})\, P_p P_A P_T / V_a \quad (8)$$

The heat Q required evaporating the water from the pad in time dt is as Equation 9:

$$Q = M_T h_{fg} = h_{fg} h_D M_w \rho_a V_a/(R_o T_{abs}) \times (P_{vs} - P_{va})\, P_p P_A P_T / V_a \quad (9)$$

where $h_{fg} = 2.503 \times 10^6 - 2.38 \times 10^3 (T_{abs} - 273.16)$ for a temperature equal to:

273.16≤T(K)≤338.723 (Dzivama 2000).

At equilibrium, equating Equation 8 and Equation 9 give Equation 10:

$$T_p = T_o db - \frac{(h_{fg}M_w(P_{vs}-P_{va})) \times Va^2 \rho a^2 (C_a + W_o C_v) \times (P_p P_A P_T)}{R_o T_{abs} \rho_a C_a (sc/pr)^{2/3} V_a} \quad (10)$$

where $\rho_a C_a (sc/pr)^{2/3}$ = h'/h_D = the ratio of the convective heat transfer to that of the mass transfer coefficient. See Equation 11 and Equation 12.

$$T_{x=L} = \frac{T_o}{v}\left(1 - e^{-vL}\right) + T_p e^{-vL} \quad (11)$$

Now

$$T = \frac{1}{L}\int_0^L T dx = \frac{T_o}{v}\left[1 - \frac{1-e^{-vL}}{vL}\right] + T_p \frac{1-e^{-vL}}{vL} \quad (12)$$

Kachhwah and Suhas (2010), presented a set of equations (from Equation 13 to Equation 22) for the inlet and outlet water temperatures associated with the evaporative cooling process. These temperatures are based on an elevated inlet water temperature entering the absorbent materials above that of the ambient wet bulb temperature. The correlation presented for heat transfer is given as:

$$Nu = y \times (Re^{0.8}) \times (Pr^{0.33}) \quad (13)$$

where $y = 0.1 \times (D_e^{0.12})$

$$\text{Reynold number,} \quad Re = \frac{\rho a \times \mu \times D_e}{\mu_a} \quad (14)$$

$$\text{Prandtl number,} \quad Pr = \frac{c_{pa} \times \mu_a}{K_a} \quad (15)$$

$$P_a = \frac{P_{atm}}{287.08 \times Twb} \quad (16)$$

$$De = \frac{V}{A} \quad (17)$$

$$\alpha = \frac{Tw - Twb}{Tdb - Twb} \quad (18)$$

$$NTU = \frac{hc \times A_s}{m_a \times c_{pa}} \quad (19)$$

$$\phi = 1 - \exp(-1.07(NTU)^{0.295}) \times \alpha^{-0.556} \times M_r^{-0.051} \quad (20)$$

The exit Tdb is calculated as

$$\eta = \phi\eta_1 \quad (21)$$

where $\eta 1 = 1 - \exp(-1.037NTU)$ (22)

The humidity ratio is calculated as Equation 23:

$$w_2 = \frac{0.62198P_{wv2}}{P_{atm} - P_{wv2}} \quad (23)$$

The equations below (from Equation 24 to Equation 26) describe the effects of the independent variables (pad thickness, air velocity and water flow rate) on the storage chamber temperature.

$$T_c = 3160.7P_T^2 - 399.79P_T + 31.54 \quad (24)$$

$$T_c = 3.0504 + 56.643\ V_a - 62.2\ V_a^2 + 26.933\ V_a^3 - 4\ V_a^4 \quad (25)$$

$$T_c = 0.2542W_R^4 - 2.8167\ W_R^3 + 11.14\ W_R^2 - 17.796\ W_R + 28.449 \quad (26)$$

where M_a is the mass of air, ρ_a is the density of air, T_o is the inlet air temperature, T_o (wb) is the wet-bulb temperature of the region, W_o is the humidity ratio of the air, M_r is the water to air mass flow rate ratio, T_{w1} is the inlet water temperature, T_{w2} is the outlet water temperature, T_{db1} is the inlet air dry bulb temperature, *Pva* is the partial vapour pressure of air, *Pvs* is the vapour pressure of saturated air at the wet-bulb at the temperature of the region, P_{atm} is the atmospheric pressure, *Cv* is the specific heat capacity of water vapour, *Ca* is the specific heat capacity of air, *Ro* is the universal gas constant, h_{fg} is the latent heat of vaporization, *Pa* is the density of air, the molecular weight of water ratio of the convective heat and mass transfer is given by $(h_1/h_D) = (sr/pr)^{2/3}$, P_T'' is the pad thickness, *Pp* is the pad porosity, P_A is the pad surface area, *Va* is the air velocity and W_R is the water flow rate. A detailed algorithm to solve the mathematical formulae is shown in Figure 2.

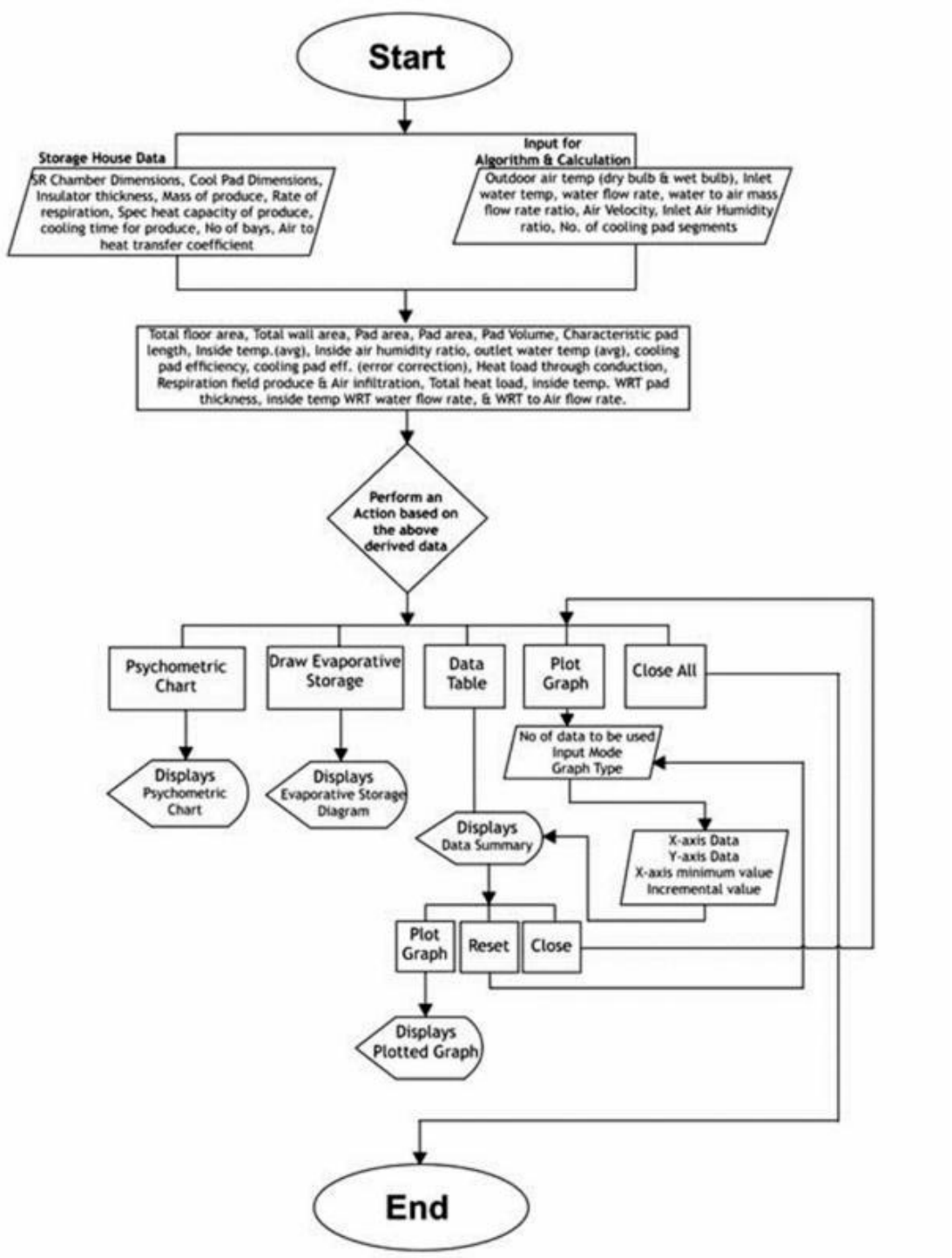

Figure 2 Flow chart for simulation algorithm

2.1.4 Description of the computer programme

The system is divided into three (3) sub systems with three different user interfaces. Three popup windows will appear after the user enters ‘cool’ in the command window of the program. Figure 3 to Figure 5 show the content of these three windows. The first window as shown in Figure 3, is used to input and calculate the dimensions of the storage chamber and the cooling pad. Lines below the ‘Derived’ section as shown in Figure 3, are the calculated results of the total floor area and the wall area, in both SI and Imperial units.

Figure 3 The First window for the storage chamber and heat load data

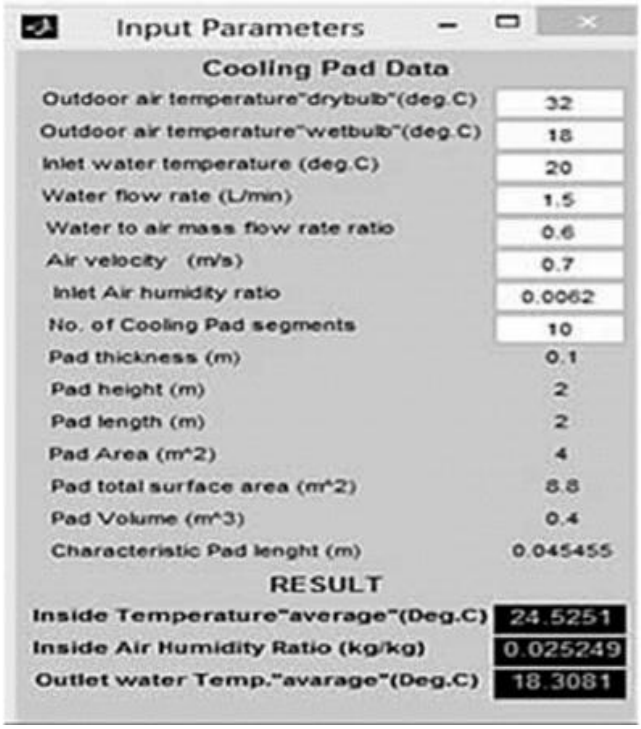

Figure 4 The Second window algorithm for dimension psychrometric entrance air data and pad data

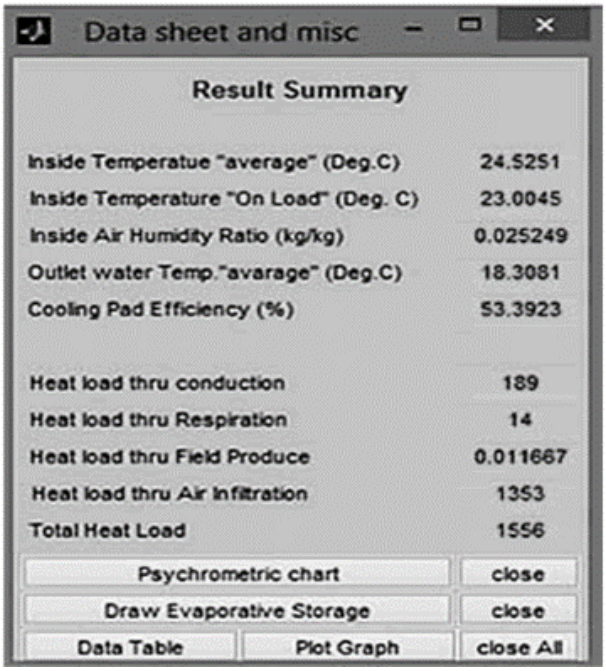

Figure 5 The Third window shows summary of characteristics of the humidified air in the storage chamber

Figure 4 shows the second window for the input of data of the psychrometric properties of air and water passing through the pad. Based on the input data, the program will calculate the related values of the storage chamber temperature, storage chamber humidity ratio and outlet water temperature.

Figure 5 shows a result window with adiabatic cooling values, a simulation of the internal air conditions in the storage chamber, and the evaporative cooling system performance efficiency. The first button calls up a digital psychrometric chart to check the outdoor wet bulb and dry bulb temperature with respect to the inlet air humidity ratio, as shown in Figure 6. The 'close' button closes the figure created by the 'Draw Evaporative Storage' option as shown in Figure 7. If the figure is not closed, then the program automatically saves all the current values as defaults for next 'run'. The 'Draw Evaporative Storage' option makes use of some parameters listed in Figure 5 to draw the storage chamber layout. The 'Data Table' buttons enable the user to recover the data generated in the last run.

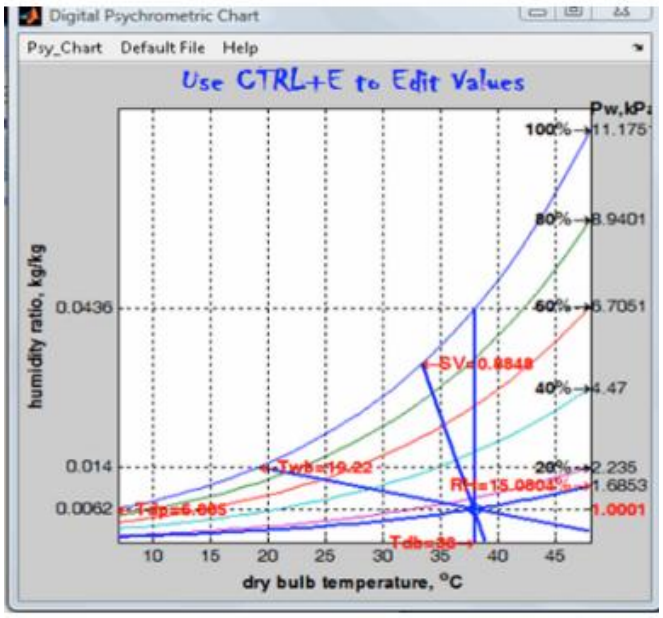

Figure 6 The Fourth window shows digital psychrometric chart

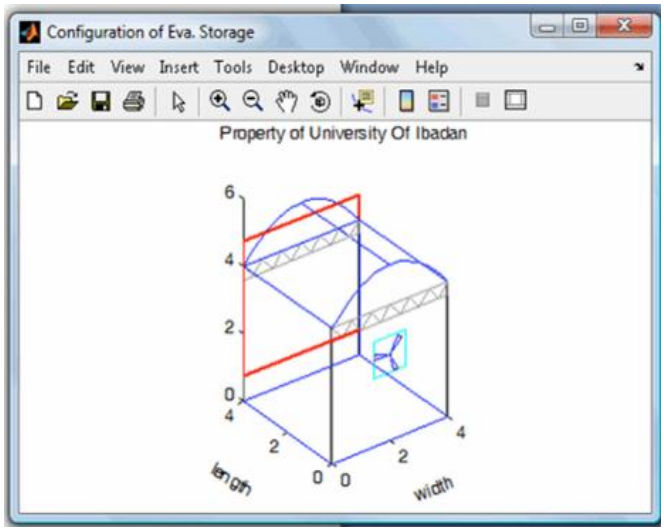

Figure 7 Evaporative cooling system storage layout

2.2 Experimental setup

For verification of the above mentioned model, the solar power evaporative system as reported by Olosunde et al. (2016) was used. The evaporative cooler consisted of a pad end, a suction fan, a storage cabin, a water pump, an overhead tank, a collection tank and pipes. The pad was installed on one side of the cabin, and the suction fan installed on the other side, opposite to the pad end. An overhead tank was installed on the top of the cooler, from which water dripped onto the pad through a lateral pipe laid on top of the pad. There was a collection tank at the bottom of the cooler to collect excess water from the pad. The pump re-circulated the excess water back to the overhead tank. The framework was of five different thicknesses of 20, 40, 60 80 and 100 mm of size 600 x 1130 mm, corresponding to one side of the storage cabin. See Figure 8.

Figure 8 Solar powered evaporative cooling storage system

2.3 Analysis

A two-sample *t*-test using pooled variance was performed to test if the hypothesis that the resulting means of the modelled data and of the experimental data were equal.

3 Results and discussion

3.1 Effect of the thickness of the pad on saturation efficiency

The effect of pad thickness on the storage chamber temperature is shown in Figure 9. A cooling pad thickness of 0.01 - 0.110 m was used to run the software. The saturation efficiency increased as the thickness of the cooling pad increased (0.01 – 0.066 m), and started to

decrease as the cooling pad thickness increased further from 0.066 – 0.11 m. This change occurred because an increase in the thickness of the pad tended to increase the residence time of the air within the pad, thus creating a longer period for the air-water contact. This phenomenon meant that the air could possibly evaporate more water due to the longer distance travelled and the residence time. However, with a further increase in the pad thickness, the air would become closer to being saturated as it travelled through the pad, which would reduce the capacity of the air to evaporate and absorb a greater amount of water from the pad. Therefore, the efficiency decreased with a greater pad thickness.

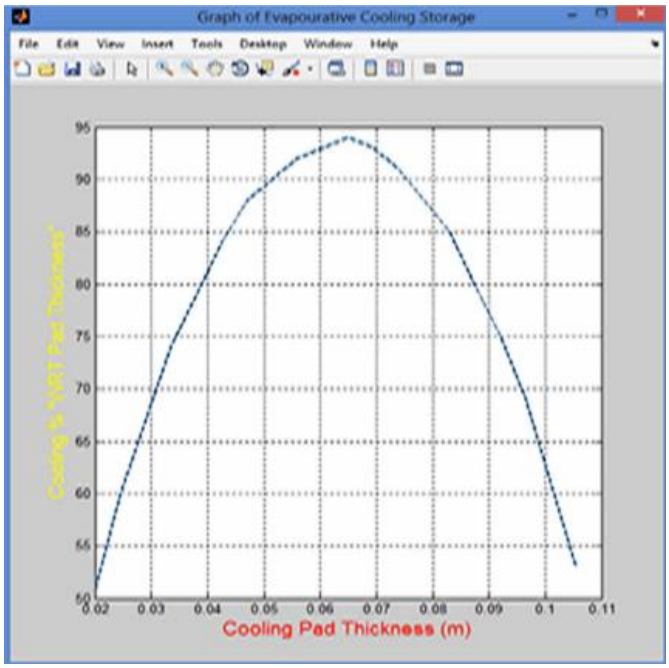

Figure 9 Effect of pad thickness on the saturation efficiency

3.2 Effect of inlet water temperature on the saturation efficiency

The effect of water temperature on the saturation efficiency is presented in Figure 10. At inlet, water temperature was between 17 ℃ and 18 ℃ and there was a sudden increase in the saturation efficiency, while a further increase in inlet water temperature beyond 18 ℃ resulted in a sudden drop in the efficiency. The sudden increase occurred because the inlet water temperature was lower than the wet bulb temperature. This result clearly indicated that the performance of the evaporative cooling was higher when the inlet water temperature was close to the wet bulb temperature.

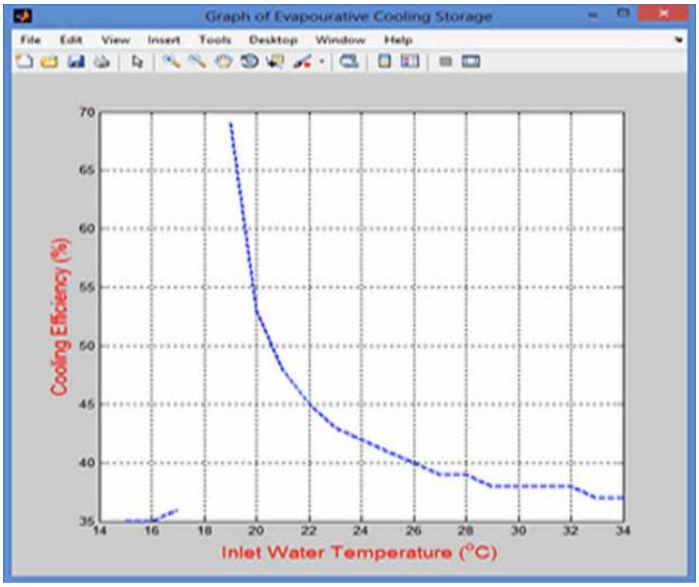

Figure 10 Effect of inlet water temperature on the saturation efficiency

3.3 Effect of air velocity on the saturation efficiency

As the air velocity increased from 0.5 to 1.7 m/s, the saturation efficiency increased. Between an air velocity of 1.7 to 1.85 m/s, the efficiency remained constant. A further increase in the air velocity reduced the efficiency as shown in Figure 11. The initial high rate of increase in the saturation efficiency with increasing air velocity due to the turbulent nature of the airflow at a high velocity within the pad, i.e., the air could evaporate more water and thus increase the efficiency. Air moving at a low velocity would not be turbulent and only evaporate the water in its path, which reduced the amount of water that could be evaporated and hence reduced the efficiency of the cooling system. However, a high velocity may reduce the residence time of the air within the pad, which resulted in a slight decline in the efficiency as the air velocity increased further. A higher velocity tended to pull water droplets out of the pad instead of evaporating them, and this effect reduced the efficiency of the system. These results are in agreement with the software prediction.

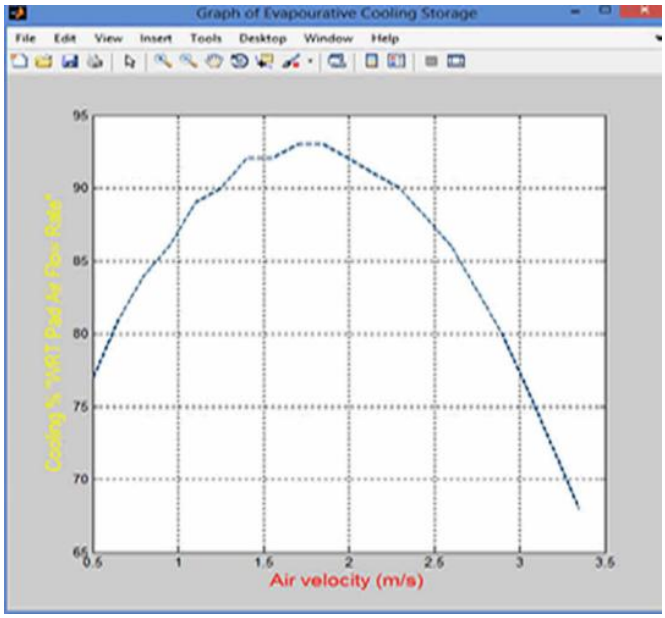

Figure 11 Effect of air velocity on the saturation efficiency

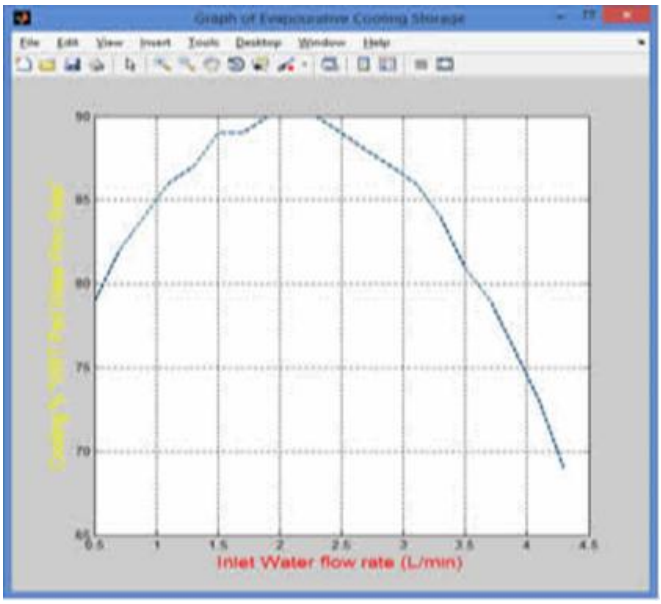

Figure12 Effect of water flow rate on the saturation efficiency

3.4 Effect of water flow rate on the saturation efficiency

Figure 12 shows the effect of the water flow rate on the saturation efficiency. The saturation efficiency increased with an increase in the water flow rate, which was obvious because a low water flow rate would leave a dry spot where unsaturated air could pass directly through the pad without evaporating water, thus increasing the storage chamber temperature and reducing the efficiency. The water may be inadequate to wet and saturate the pad. As the water flow rate increases, the pad becomes wet and closer to being saturated, i.e., the air evaporated more water from the pad and, therefore, more cooling occurred. The value of the saturation efficiency was observed to decline slightly after a water flow rate of 2 L/min, because at this flow rate the pad was excessively wet with water. The excess water may block the pore spaces within the pad fibres, thereby impeding the free flow of air through the pad which reduced good evaporation.

3.5 Comparison between the modelled data and the experimental data of the four parameters of the saturation efficiency

The hypotheses for this test are H_0: $\mu_1 = \mu_2$ versus *Ha*: $\mu_1 \neq \mu_2$ or, in words, the following:

Null hypothesis (H_0): There is no significant difference between the experimental data and the simulated data of the effects of Pad thickness, air velocity, water flow rate and water temperature on the saturation efficiency.

Alternative hypothesis (*Ha*): There is a significant difference between the experimental data and the simulated data of the effects of Pad thickness, air velocity, water flow rate and water temperature on the saturation efficiency.

Figure 13 shows a comparison between the modelled data and the experimental data of the saturation efficiency as a function of the pad thickness. From the graph no significant difference is observed between the respective mean values of the modelled and experimental data of the mean effect of the Pad thickness on the saturation efficiency, t (5) = 0.494, p = 0.635. ($p > 0.05$),- as presented in Table 1

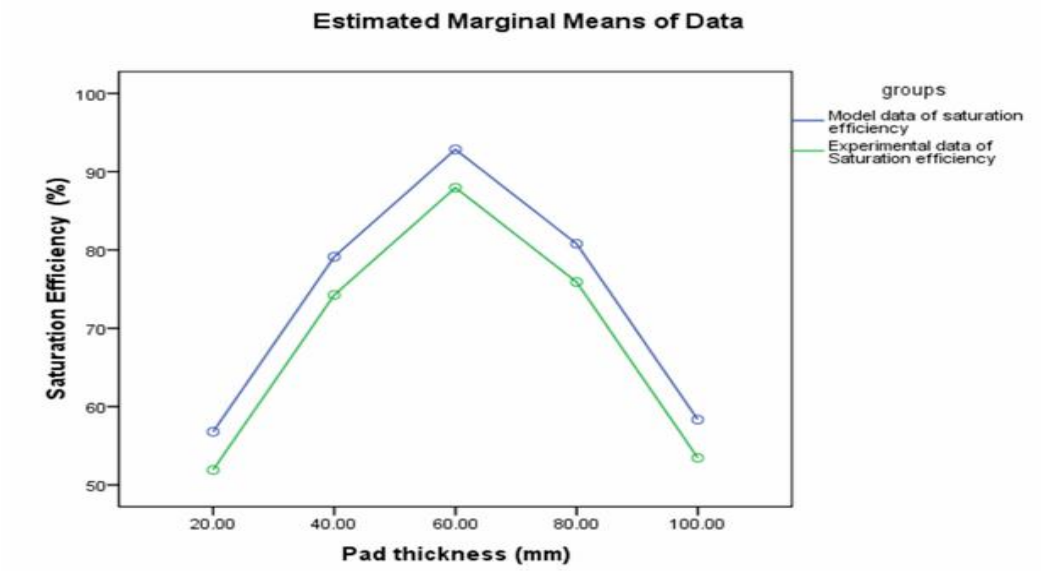

Figure 13 Comparison between modelled data and experimental data of saturation efficiency against pad thickness

Table 1 Independent samples test of the pad thickness against the modelled and experimental data of the saturation efficiency

Levene's test for equality of variance				t-test for equality of means						
								95% confidence interval		
	Equal variances	F	Sig.	t	df	Sig. 2-tailed	Mean diff.	Std error	Lower	Upper
Data	assumed	.23	.644	.494	8	.635	4.88	9.879	-17.901	27.661
	not assumed			.494	7.829	.635	4.88	9.879	-17.988	27.748

The relationship between the modelled data and the experimental data of the saturation efficiency versus the air velocity is described in Figure 14. From the graph, no significant difference was observed for the mean effect of air velocity on the saturation efficiency for the experimental data and the simulation data, t (5) = 1.639, p = 0.140. ($p > 0.05$), as presented in Table 2

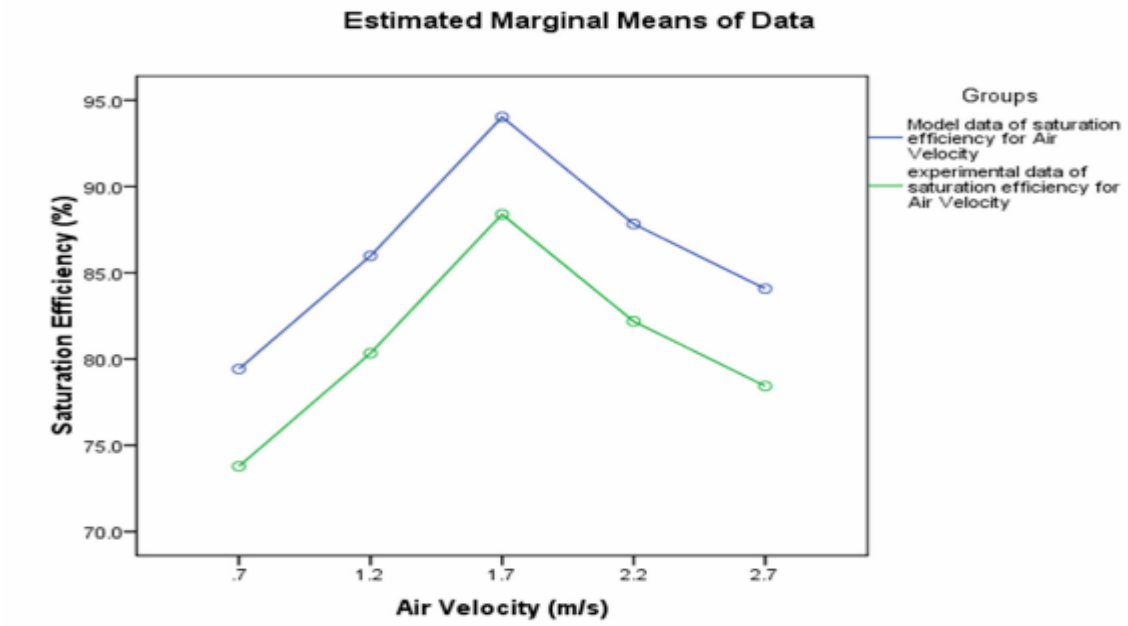

Figure 14 Comparison between modelled data and experimental data of saturation efficiency against air velocity

Table 2 Independent samples test of the air velocity against the modelled and the experimental data of the saturation efficiency

	Levene's test for equality of variance			t-test for equality of means					95% confidence interval	
	Equal variances	F	Sig.	t	df	Sig. 2-tailed	Mean diff.	Std error	Lower	Upper
Data	assumed	.261	.624	1.64	8	.140	5.64	3.442	-2.297	13.577
	not assumed			.494	7.41	.143	5.64	3.442	-2.407	13.687

Additionally, the relationship between the modelled data and the experimental data of the saturation efficiency versus the water flow rate is described in Figure 15. From the graph, no significant difference was found between the modelled and experimental mean values. Thus, the mean effect of the water flow rate on the saturation efficiency for both the experimental data and the simulation data were not significantly different, t (5) = 1.013, p = 0.341. ($p > 0.05$),- see Table 3 for the details.

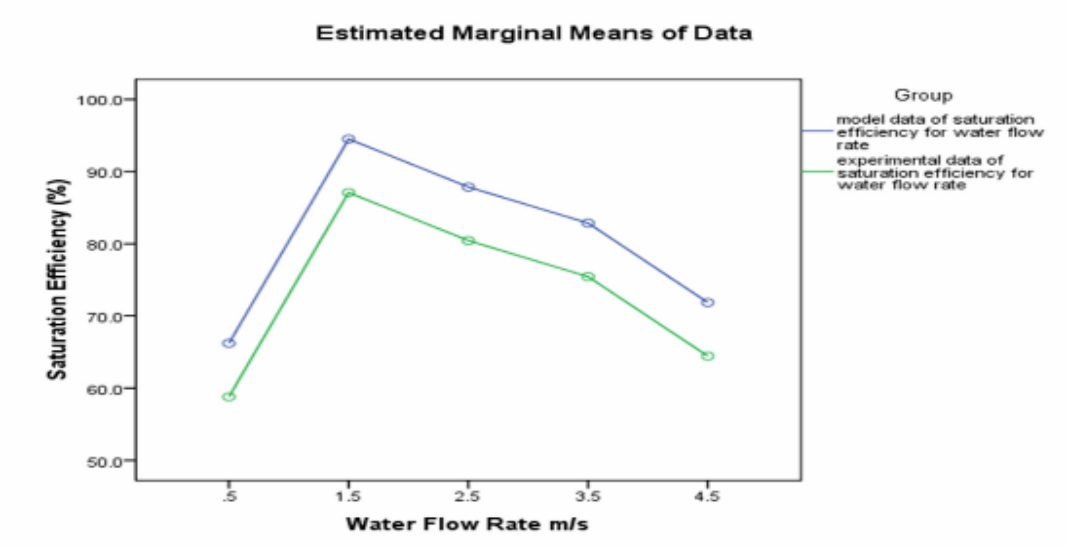

Figure 15 Comparison between modelled data and experimental data of saturation efficiency against water flow rate

Table 3 Independent samples test of the water flow rate against the modelled and the experimental data of the saturation efficiency

	Levene's test for equality of variance			t-test for equality of means					95% confidence interval	
	Equal variances	F	Sig.	t	df	Sig. 2-tailed	Mean diff.	Std error	Lower	Upper
Data	assumed	.020	.891	1.013	8	.341	7.42	7.326	-9.473	24.313
	Not assumed			1.013	7.99	.341	7.42	7.326	-9.476	24.316

Figure 16 shows the relationship between the modelled data and the experimental data of the saturation efficiency versus water temperature. From the graph, no significant difference was observed between their respective mean values. Thus, the mean effect of water temperature on the saturation efficiency for both the experimental results and the simulation result were not significantly different, t (5) = -0.597, p = 0.567. ($p > 0.05$),- see Table 4 for the details.

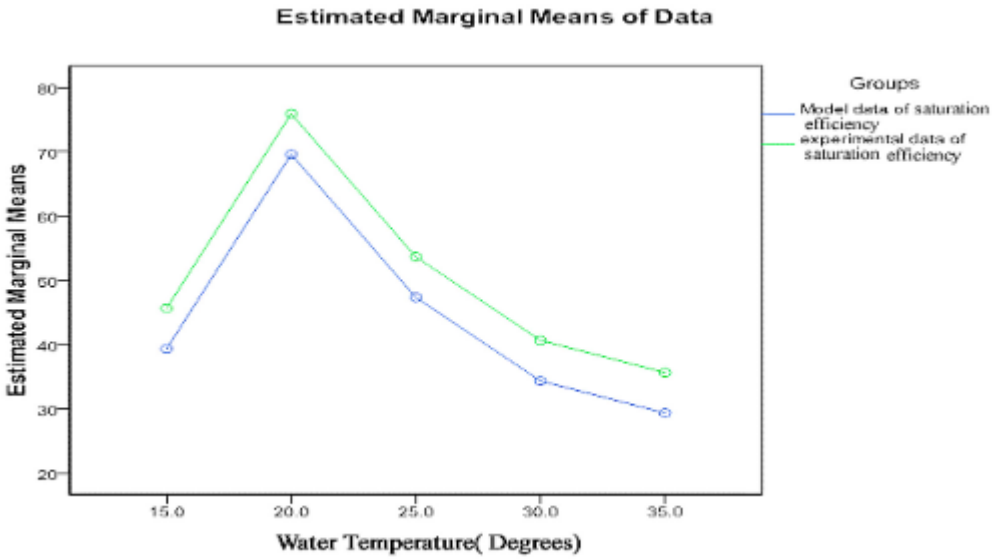

Figure 16 Comparison between modelled data and experimental data of saturation efficiency against water temperature

Table 4 Independent samples test of the water temperature against the modelled and the experimental data of the saturation efficiency

Levene's test for equality of variance				t-test for equality of means						
									95% confidence interval	
	Equal variances	F	Sig.	t	df	Sig. 2-tailed	Mean diff.	Std error	Lower	Upper
Data	assumed	.357	.567	-.597	8	.567	-6.30	10.55	-30.63	18.027
	not assumed			-.597	7.63	.568	-6.30	10.55	-30.84	18.237

4 Conclusions

The developed program is simple and efficient, with a suitable interface for the input of the necessary data, and the program provides sufficient information to optimize the design of an evaporative cooling system for the storage of fruits and vegetables. The results of the comparison between the modelled data and the experimental data indicated that there was no significant difference between the software generated data and the experimental data of the saturation efficiency versus Pad thickness – mm ($p = 0.635$), Air Velocity - m/s ($p = 0.140$), Water Flow Rate - L/min ($p = 0.341$) and Water Temperature ^{0}C ($p = 0.567$) at $\alpha = 0.05$ significant level and 95 % confidence interval.

Hence, the program provides the capability to identify the working conditions based on the appropriate figures, thus demonstrating the effect of the cooling pad thickness, water flow rate, inlet water temperature, air velocity, number of cooling segments and water to air flow rate on the storage chamber temperature, the storage chamber humidity ratio and the saturation efficiency.

References

Boyette, M. D., L. G. Wilson, and E. A. Estes. 2010. Postharvest handling and cooling of fresh fruits, vegetables and flowers for small farms. Leaflets 800-804. North Carolina Cooperative Extension.

Camargo, J. R., C. D. Ebinuma, and S. Cardoso. 2003. A mathematical model for direct evaporative cooling air conditioning systems. *Engenharia Termica, Curitiba*, 4(1):30-34.

Cui, X., K. J. Chua, and W. M. Yang. 2014. Use of direct evaporative cooling as pre-cooling unit in humid tropical climate: an energy saving technique. The 6th International Conference on Applied Energy – ICAE 2014. *Energy Procedia*, 61(2014):176-179. doi:10.1016/j.egypro.2014.11.933.

Dzivama, A.U. 2000. Performance evaluation of an active cooling system for the storage of fruits and vegetables. Ph.D. Thesis, Department of Agricultural Engineering, University of Ibadan, Ibadan.

Fang, W., D. S. Fon, Z. H. Jian, and D. C. Wang. 2001. Re-development of Psychrometric software using Visual C++ and MATLAB. *Proceedings of the International Forum for Vegetable Production*. Amen, China.

Kachhwah, S. S., and P. Suhas. 2010. Heat and mass transfer study in a direct evaporative cooler. *Journal of Scientific and Industrial Research,* 69(9):705-710.

Kulkarni, R. K., and S. P. S. Rajput. 2011. Comparative performance of evaporative cooling pads of alternative materials. *International Journal of Advanced Engineering Sciences and Technologies,* 10(2):239-249.

Ndukwu, M. C., and S. I. Manuwa. 2014. Review of research and application of evaporative cooling in preservation of fresh agricultural produce. *International Journal of Agricultural and Biological Engineering*, 7(5):85-102.

Ndukwu, M. C., S. I. Manuwa, O. J. Olukunle, and I. B. Oluwalana. 2013. Development of an active evaporative cooling system for short-term storage of fruits and vegetables in a tropical climate. *Agricultural Engineering International: CIGR Journal*, 15(4):307-313.

Ndukwu, M. C. 2011. Development of a clay evaporative cooler for fresh fruits and vegetables preservation. *Agricultural Engineering International: CIGR Journal*, 13(1):1-8.

Olosunde, W. A., A. K. Aremu, and D. I. Onwude. 2016. Development of a solar powered evaporative cooling storage system for tropical fruits and vegetables. *Journal of Food Processing and Preservation*, 40(2):279-290

Olosunde, W. A. 2015. Performance of a forced convection evaporative cooling storage system for selected tropical perishable crops. Ph.D. Thesis, Department of Agricultural Engineering, University of Ibadan, Ibadan.

Olosunde, W. A., J. C. Igbeka, and T. O. Olurin. 2009. Performance evaluation of absorbent materials in evaporative cooling system for the storage of fruits and vegetables. *International Journal of Food Engineering*, 5(3):1-15.

Sirelkhatim, A. K. and A. A. Emad. 2012. Improvement of evaporative cooling system efficiency in greenhouses. *International Journal of Latest Trends in Agriculture and Food Sciences*, 2(2):83-89.

Taye, S. M. and P. F. Olorunisola. 2011. Development of an evaporative cooling system for the preservation of fresh vegetables. *African Journal of Food Science*, 5(4):255-266.

Van der Walt, N. T., and R. Hemp. 1989. Thermometry and temperature measurements in environmental engineering in South African Mines. Chp 17. The Mine Ventilation Society of South Africa.

Wang, D. C., W. Fang, and D. S. Fon. 2002. Development of a digital psychrometric calculator using MATLAB. *Acta Horticulturae,* 578:339-344. DOI: 10.17660/ActaHortic.2002.578.42

Wei, Z., and S. Geng. 2009. Experimental research on direct evaporative cooling of organic padding contamination. *Contamination Control & Air-Conditioning Technology*, 22-26.

Xuan, Y. M., F. Xiao, X. F. Niu, X. Huang, and S. W. Wang. 2012. Research and application of evaporative in China: A review (I). *Renewable and Sustainable Energy Reviewers*, 16(5):3535-3546.